Research Article Vol. 31, No. 5 / 27 Feb 2023 / Optics Express 8240
Optics EXPRESS

Optomechanics and quantum phase of the Bose-Einstein condensate with the cavity mediated spin-orbit coupling

PENG ZHANG,[1] PENGJU TANG,[2,3,4] RUIZHI PAN,[2,5] XUZONG CHEN,[2] XIAOJI ZHOU,[2,6,7] AND SHOUGANG ZHANG[1,8]

[1]Key Laboratory of Time and Frequency Primary Standards, National Time Service Center, Chinese Academy of Sciences, Xi'an 710600, China
[2]State Key Laboratory of Advanced Optical Communication System and Network, School of Electronics, Peking University, Beijing 100871, China
[3]China Academy of Electronics and Information Technology, Beijing 100041, China
[4]Yangtze Delta Region Industrial Innovation Center of Quantum and Information Technology, Suzhou 215000, China
[5]Joint Quantum Institute, NIST/University of Maryland, College Park, Maryland 20742, USA
[6]Institute of Advanced Functional Materials and Devices, Shanxi University, Taiyuan 030031, China
[7]xjzhou@pku.edu.cn
[8]szhang@ntsc.ac.cn

Abstract: We investigated the optomechanical dynamics and explored the quantum phase of a Bose-Einstein condensate in a ring cavity. The interaction between the atoms and the cavity field in the running wave mode induces a semiquantized spin-orbit coupling (SOC) for the atoms. We found that the evolution of the magnetic excitations of the matter field resembles that of an optomechanical oscillator moving in a viscous optical medium, with very good integrability and traceability, regardless of the atomic interaction. Moreover, the light-atom coupling induces a sign-changeable long-range interatomic interaction, which reshapes the typical energy spectrum of the system in a drastic manner. As a result, a new quantum phase featuring a high quantum degeneracy was found in the transitional area for SOC. Our scheme is immediately realizable and the results are measurable in experiments.

1. Introduction

Cavity quantum electrodynamics (CQED) describes the coherent interaction between matter fields and electromagnetic (EM) fields within optical resonators. In the CQED systems, the dynamics of the matter field and that of the EM field greatly affect each other [1,2]. Cavity optomechanics is one of the good examples studying the coupling between a quantum mechanical oscillator and the EM field inside a cavity [3–5]. It has been a continually refreshing subject in cold atom physics. Through the combination of CQED and cold atom physics, a wide range of exotic quantum phenomena have been investigated. In the past few years, there has been a breakthrough in realizing the spin-orbit coupling (SOC) in cold atom gases [6–8] which could be naturally incorporated into the CQED systems. Perspectives of new quantum kinetics and fascinating phenomena are being opened up in the relevant areas like realizing quantum systems with synthetic dimensions [9], ideal Weyl semimetal [10], and superradiant phase transition [11].

In the experiments of the ultracold atomic gases with the SOC in open space, the coupling between the atomic spin (or pseudo spin) and the center of mass (c. m.) motion is induced by utilizing the classical Raman laser beams [6–8] that are far-detuned with the atomic resonance frequencies. Then the coupling between lights and atoms is weak; thus the fluctuation of the light fields is negligible. However, when the atoms are placed inside the cavity, the atoms can exert a strong influence on the cavity field; thus strong nonlinear effects would arise [12–15]. Meanwhile,

#477780 https://doi.org/10.1364/OE.477780
Journal © 2023 Received 24 Oct 2022; revised 26 Dec 2022; accepted 9 Jan 2023; published 21 Feb 2023

Optics EXPRESS

because all the atoms couple to the same cavity field, a long-range atomic correlation could be induced. With the help of optical resonators, different kinds of cavity-mediated long-range atomic interactions have been realized in investigations on dynamical phase transitions [16], Spin Entanglement [17], superradiant quantum phase transition [18], etc. Such nonlinearity and long-range correlation generate many intriguing effects that are unique in the CQED systems.

This paper is devoted to the study of optomechanics and the rich quantum phase of a Bose-Einstein condensate (BEC) contained in a ring cavity in which a light in the running wave mode is maintained. It is a typical CQED system that can generate a semiquantized SOC for the atoms [2,19]. We are going to show that this system is an optomechanical system and that the optomechanical kinetics of the matter wave excitations is highly integrable and traceable. This is a valuable merit in contrast to the previous works [6,7,14,20]. Moreover, it has been demonstrated that CQED systems with SOC can have very rich quantum phases [19,21] and complex dispersion relations [2]; and along with these phenomena, there is the typical double-minima to single-minimum transition in the energy dispersion relation. However, due to the presence of the long-range correlation among the atoms induced by the SOC in the cavity, a new quantum phase with high quantum degeneracy will appear at the transition point. The latter part of this work is to uncover this new phase. This paper is organized as the following: In Section 2, we present the principal model and theory of the CQED system with the SOC. In Section 3, we study the properties of the optomechanical motion of the magnetic excitations of the system. In Section 4, we demonstrate a detailed analysis of the spectrum of the elementary excitations and present the phase diagram of the magnetic order of the matter field, in which the new quantum phase is included. Finally, in Section 5, we give a discussion and summary of our results.

2. Description of the system and the model

Consider a BEC trapped in a triangular ring cavity as shown in Fig. 1(a) [22–24]. The BEC is prepared with atoms with a Λ-type energy level structure as shown in Fig. 1(b). A driving field of frequency ω_d is pumped into the cavity to excite a running light in the counterclockwise cavity mode with a wavevector $-\mathbf{k}_c$ and frequency ω_c. At the same time, another coherent laser beam with a wavevector $\mathbf{k}_p$ and frequency ω_p is applied to intersect the cavity field; and the BEC is trapped right at the intersecting region of the light fields. A magnetic field $\mathbf{B}$ is used to tune the Zeeman splitting energy of the atoms. By tuning the frequencies of these light fields, we can select out one pair of atomic internal states $|\pm\rangle$ that are closely resonant with each other with only a small energy difference h as shown in Fig. 1(b). In order to make a specific illustration, we take the ^{87}Rb atoms used in real experiments [25,26] as an example. The σ^- laser field with frequency ω_p couples the spin-up state $|F, m_F\rangle = |2, -2\rangle \equiv |+\rangle$ with an excited state, and the π cavity field with frequency ω_c couples the excited state with the spin-down state $|F, m_F\rangle = |1, -1\rangle \equiv |-\rangle$. ω_c and ω_p should be far off-resonant with the energy differences of the corresponding quantum transitions to avoid heating up the atoms. In such a situation, the excited state can be adiabatically eliminated [27,28]. Therefore, the states $|\pm\rangle$ can describe the spin order of the system well.

The Hamiltonian of the light-atom coupling system is ($\hbar = 1$) [2,23]

$$\begin{aligned}\hat{H} = {} & \omega_c \hat{a}^\dagger \hat{a} + \sum_\sigma \int d\mathbf{x} \hat{\Psi}_\sigma^\dagger(\mathbf{x}) \left(-\frac{1}{2M}\nabla^2 + \zeta_\sigma \cdot \frac{\Delta_B}{2} \right) \hat{\Psi}_\sigma(\mathbf{x}) \\ & + \Omega \left(\int d\mathbf{x} \hat{\Psi}_-^\dagger(\mathbf{x}) \hat{\Psi}_+(\mathbf{x}) \hat{a} e^{i\omega_p t + i\mathbf{k}_r \cdot \mathbf{x}} + c.c. \right) \\ & + \frac{g}{2} \sum_{\sigma\sigma'} \int d\mathbf{x} \hat{\Psi}_\sigma^\dagger(\mathbf{x}) \hat{\Psi}_{\sigma'}^\dagger(\mathbf{x}) \hat{\Psi}_{\sigma'}(\mathbf{x}) \hat{\Psi}_\sigma(\mathbf{x}) \\ & + i2\eta \cos(\omega_d t) \left(\hat{a}^\dagger - \hat{a} \right) - i\kappa \hat{a}^\dagger \hat{a},\end{aligned} \tag{1}$$

Optics EXPRESS

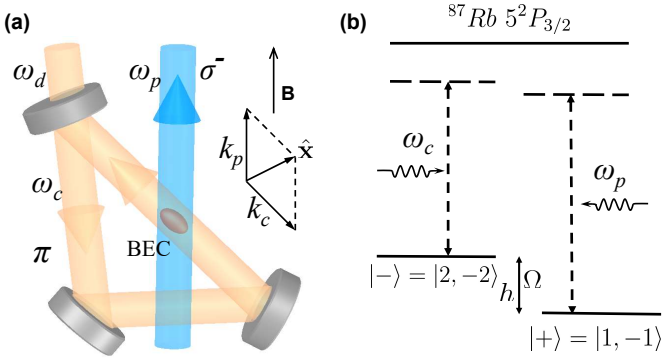

Fig. 1. (a) The schematic diagram of a Bose-Einstein condensate interacting with a traveling wave mode of a ring cavity and a pump field. (b) The energy level structure of the atom. h is the two-photon Raman detuning including the Zeeman splitting energy difference between the two spinor states in the rotated frame. Ω is the effective Rabi frequency for the two spinor states being coupled through the two-photon Raman processes.

where the first line is the noninteracting Hamiltonian of the CQED system. $\hat{a}^\dagger$ ($\hat{a}$) is the photon creation (annihilation) operator of the cavity field to create (annihilate) photons in the counter-propagating mode of the ring cavity. M is the mass of a single atom. $\hat{\Psi}^\dagger_\sigma(\mathbf{x})$ and $\hat{\Psi}_\sigma(\mathbf{x})$ (with $\zeta_\sigma = \pm 1$ for $\sigma = \mp$) are the creation and annihilation operators of the matter field for the corresponding spin states $|\pm\rangle$. Δ_B is the Zeeman splitting energy between the $|-\rangle$ and $|+\rangle$ states, in which both the linear and quadratic Zeeman splitting effects have been included [7]. The second line describes the light-atom coupling, in which the symbol "$c.c.$" means the complex conjugation. Ω is the two-photon Rabi-frequency; and without the loss of generality, it is chosen to be real. We define the quantity k_r in this way: When the cavity field exchanges one photon with the classical pump field through the matter field, the momentum of the matter field is changed by $\pm 2k_r$; then by defining $\mathbf{k}_r \equiv \frac{1}{2}\left(\mathbf{k}_p + \mathbf{k}_c\right)$, we have $k_r = |\mathbf{k}_r|$. In the following discussions, $|\mathbf{k}_p|$ and $|\mathbf{k}_c|$ are taken to be identical with each other despite the existence of a frequency difference between the different light fields due to the dispersion relation of light. The intersecting angle between $\mathbf{k}_p$ and $\mathbf{k}_c$ is adjustable; and for the sake of simplicity, it is chosen to be 120° so that $k_r = \frac{1}{2}k_p$. The third line is the interparticle interaction of the matter field, which can be recast into the expression composed of observable quantities

$$\hat{H}_{int} = \frac{g}{2}\int dx\,(\hat{n}_-(\mathbf{x}) + \hat{n}_+(\mathbf{x}))^2\,,$$

where $\hat{n}_\pm(\mathbf{x}) = \hat{\Psi}^\dagger_\pm(\mathbf{x})\hat{\Psi}_\pm(\mathbf{x})$ are the local atomic density operators. The parameter $g = \frac{4\pi a_s}{M}$, with a_s being the s-wave scattering length, characterizes the strength of the atomic contact interaction. Finally, the first term in the last line represents a driving term from the driving field pumping photons into the cavity at a rate η; and the second term is a phenomenological term describing the leakage of photons out of the cavity at a rate κ.

The Hamiltonian (1) is time-dependent. We can remove this time dependence in the rotating frame by using the rotating wave approximation (RWA) to eliminate the fast rotating terms. This is carried out by performing a time-dependent unitary transformation on the original system. Define

$$\hat{U}(t) = e^{-i\omega_p t\hat{a}^\dagger\hat{a} + i\sum_\sigma \frac{\zeta_\sigma}{2}\delta_p t\int d\mathbf{x}\hat{\Psi}^\dagger_\sigma(\mathbf{x})\hat{\Psi}_\sigma(\mathbf{x})}$$

Optics EXPRESS

with $\delta_p \equiv \omega_p - \omega_d$, then $\hat{H}$ becomes

$$\begin{aligned}\hat{H}' &= \hat{U}^{-1}(t)\hat{H}\hat{U}(t) - i\hat{U}^{-1}(t)\frac{d}{dt}\hat{U}(t) \\ &= \Delta_c\hat{a}^\dagger\hat{a} + \sum_\sigma \int d\mathbf{x}\hat{\Psi}^\dagger_\sigma(\mathbf{x})\left(\frac{-\nabla^2}{2M} + \zeta_\sigma \cdot \frac{h}{2}\right)\hat{\Psi}_\sigma(\mathbf{x}) \\ &+ \Omega\left(\int d\mathbf{x}\hat{\Psi}^\dagger_-(\mathbf{x})\hat{\Psi}_+(\mathbf{x})\hat{a}e^{i\mathbf{k}_r\cdot\mathbf{x}} + c.c.\right) \\ &+ \frac{g}{2}\sum_{\sigma\sigma'}\int d\mathbf{x}\hat{\Psi}^\dagger_\sigma(\mathbf{x})\hat{\Psi}^\dagger_{\sigma'}(\mathbf{x})\hat{\Psi}_{\sigma'}(\mathbf{x})\hat{\Psi}_\sigma(\mathbf{x}) \\ &+ i\eta\left(\hat{a}^\dagger - \hat{a}\right) - i\kappa\hat{a}^\dagger\hat{a}\end{aligned}$$

in the rotating frame. $\Delta_c \equiv \omega_c - \omega_d$ is the detuning of the cavity field from the driving field. For Δ_c<0, the cavity field is called red-detuned, and Δ_c>0, blue-detuned. $h = \Delta_B + \delta_p$ is the two-photon Raman detuning. In the last equality, we have taken away the terms of high frequency according to RWA. The non-interacting Hamiltonian of the matter field in $\hat{H}'$ is now

$$\hat{H}'_0 = \int d\mathbf{x}\hat{\Psi}^\dagger(\mathbf{x})\begin{bmatrix} \frac{-\nabla^2}{2M} + \frac{h}{2} & \Omega\hat{a}e^{+i\mathbf{k_r}\cdot\mathbf{x}} \\ \Omega\hat{a}^\dagger e^{-i\mathbf{k_r}\cdot\mathbf{x}} & \frac{-\nabla^2}{2M} - \frac{h}{2}\end{bmatrix}\hat{\Psi}(\mathbf{x}),$$

with the two-component spinors defined as

$$\hat{\Psi}(\mathbf{x}) \equiv \begin{bmatrix}\hat{\Psi}_-(\mathbf{x}) \\ \hat{\Psi}_+(\mathbf{x})\end{bmatrix}, \quad \hat{\Psi}^\dagger(\mathbf{x}) \equiv \left[\hat{\Psi}^\dagger_-(\mathbf{x}), \hat{\Psi}^\dagger_+(\mathbf{x})\right]. \tag{2}$$

Through introducing a local gauge transformation

$$\hat{G}(\mathbf{x}) = \begin{bmatrix} e^{-i\mathbf{k}_r\cdot\mathbf{x}} & 0 \\ 0 & e^{i\mathbf{k}_r\cdot\mathbf{x}}\end{bmatrix}, \tag{3}$$

under which $\hat{H}'$ changes to $\hat{G}(\mathbf{x})\hat{H}'\hat{G}^\dagger(\mathbf{x})$, the non-interacting Hamiltonian of the matter field becomes

$$\hat{H}_0 = \int d\mathbf{x}\hat{\Psi}^\dagger(\mathbf{x})\begin{bmatrix} \frac{(-i\nabla+\mathbf{k}_r)^2}{2M} + \frac{h}{2} & \Omega\hat{a} \\ \Omega\hat{a}^\dagger & \frac{(-i\nabla-\mathbf{k}_r)^2}{2M} - \frac{h}{2}\end{bmatrix}\hat{\Psi}(\mathbf{x}). \tag{4}$$

It is this term that bears the SOC (which will be given in an express form in the latter part of this article). The SOC generated here is semiquantized, because the cavity field that participates in the inducing of the SOC is very geometrically confined, rendering that the quantum nature of the cavity field is very prominent and thus shall not be neglected. Therefore, we have been describing the cavity field in a full quantum manner, while still treating the external laser beam as classical light in open space. This adds new features to the light-atom coupling system which is the focus of our study, in comparison with the cases of light-atom coupling in open space [6,7].

In this stage, we end up with an expression of the Hamiltonian for the whole system as

$$\hat{H} = \hat{H}_0 + \hat{H}_{int} + \Delta_c\hat{a}^\dagger\hat{a} + i\eta\left(\hat{a}^\dagger - \hat{a}\right) - i\kappa\hat{a}^\dagger\hat{a}, \tag{5}$$

where we still use the symbol $\hat{H}$ to denote the Hamiltonian of the system if there is no danger of confusion.

Optics EXPRESS

3. Optomechanical motion of the magnetic excitations

For studying the dynamics of the cavity field and the matter field we switch to the Heisenberg picture. The equations of motion of the annihilation operators of the cavity field and the matter field can be obtained as,

$$\begin{aligned} i\,\frac{\partial\hat{\Psi}(t)}{\partial t} &= \begin{bmatrix} \frac{(i\nabla-\mathbf{k}_r)^2}{2M}+\frac{h}{2}+g\hat{n}(t) & \Omega\hat{a}(t) \\ \Omega\hat{a}^{\dagger}(t) & \frac{(i\nabla+\mathbf{k}_r)^2}{2M}-\frac{h}{2}+g\hat{n}(t) \end{bmatrix}\hat{\Psi}(t), \\ i\,\frac{d}{dt}\hat{a}\,(t) &= \Delta_c\hat{a}\,(t)+\Omega\int d\mathbf{x}\hat{\Psi}_{+}^{\dagger}(t)\hat{\Psi}_{-}(t)-i\kappa\hat{a}+i\eta. \end{aligned} \tag{6}$$

It is seen that the strong coupling between the lights and atoms in the CQED system mixes the dynamics of the cavity field and the matter field together; it enhances the feedback of the atomic motion upon the cavity field and vice versa.

To simplify the discussion, we set the direction of the vector $\mathbf{k}_p + \mathbf{k}_c$ as the positive direction of the $\hat{x}$ axis. Next, we apply the mean-field approximation, which is capable of capturing the characteristics of the low-energy light-atom scattering processes, to the equations of motion of the cavity field and the matter field. By replacing the quantum operators in (6) with their classical counterparts, we obtain

$$\begin{aligned} i\frac{\partial\psi_{\pm}}{\partial t} &= \left[\frac{(-i\partial_x\mp k_r)^2}{2M}\mp\frac{h}{2}+g\cdot n\right]\psi_{\pm}+\Omega\alpha^{\pm}\psi_{\mp}, \\ i\dot{\alpha}\,(t) &= \Delta_c\alpha+\Omega\int dx\psi_{+}^{\dagger}\psi_{-}-i\kappa\alpha+i\eta, \end{aligned} \tag{7}$$

where $\psi_{\pm}$ are the wavefunctions of the two components of the matter field. $n \equiv \psi_{+}^{*}\psi_{+}+\psi_{-}^{*}\psi_{-}$ is the local atomic density. $\alpha^{+} = (\alpha^{-})^{*} = \langle\hat{a}\rangle^{*}$ is related to the quantum average of $\hat{a}$ over the state of the system. As shown in the second equation, the coupling of the two components of the matter field is of zeroth order in the cavity field amplitude [14]. Such feature distinguishes this system from other systems with the cavity field quantized as standing waves [20,29], making the optomechanical motion of the magnetic excitations of the BEC highly integrable and traceable.

The excitation of the matter field is the magnetic excitation generated in the spin-flipping processes. When the cavity field exchanges photons with the laser field through the atoms, the spins of the atoms are flipped due to the transportation of spin from the light fields to the atoms. At the same time, there is also a momentum transfer to the atoms. Therefore, the wavefunction of the excitation of the system can be characterized by a plane wave with spin.

For a BEC in the spin-up plane wave state $\tilde{\phi}_{+}^{k}(x) = \frac{1}{\sqrt{L}}e^{ikx}\otimes|+\rangle$ with momentum k (where L is the volume of the system), the cavity field, together with the pump field, couples it to the state $\tilde{\phi}_{-}^{k+2k_r}(x) = \frac{1}{\sqrt{L}}e^{i(k+2k_r)x}\otimes|-\rangle$. At this time, we need to bear in mind that we shall be working in the rotated frame, in which $\tilde{\phi}_{+}^{k}(x)$ and $\tilde{\phi}_{-}^{k+2k_r}(x)$ become

$$\begin{aligned} \phi_{+}^{k}\,(x) &= \hat{G}\tilde{\phi}_{+}^{k}(x) = \frac{1}{\sqrt{L}}\begin{bmatrix} 0 \\ e^{i(k+k_r)x} \end{bmatrix}, \\ \phi_{-}^{k+2k_r}\,(x) &= \hat{G}\tilde{\phi}_{-}^{k+2k_r}(x) = \frac{1}{\sqrt{L}}\begin{bmatrix} e^{i(k+k_r)x} \\ 0 \end{bmatrix}, \end{aligned} \tag{8}$$

under the local gauge transformation (3). Here, we have introduced the column vectors $[0,1]^T$ and $[1,0]^T$ to represent the spin-up state and spin-down state, respectively.

Optics EXPRESS

Now we use the family $\{\phi_+^k(x), \phi_-^k(x)\}$ to expand wavefunction of the matter field

$$\psi(x,t) = \sum_k \left\{c_-^k(t)\,\phi_-^k(x) + c_+^k(t)\,\phi_+^k(x)\right\}, \tag{9}$$

where k is the quasi-momentum of each plane wave component. $\psi(x,t) = [\psi_-(x,t), \psi_+(x,t)]^T$ is the wavefunction of matter field. The probability amplitudes $c_\pm^k$ are normalized in the way such that $\sum_k\{|c_-^k|^2 + |c_+^k|^2\} = N$, where N is the atom number.

Consider a BEC that is prepared in the spin-up state $\phi_+^0(x)$, and initially stationary. We assume that the BEC is dilute, thus the interatomic interaction is weak and can be neglected, so is its modification upon the c. m. motion of the atoms. In this condition, the relations $|c_-| \ll |c_+|$ and $|\dot{c}_-| \gg |\dot{c}_+|$ hold.

Define

$$X \equiv N^{-\frac{1}{2}}\int dx\psi_+^*(x)\,\psi_-(x) = \frac{1}{\sqrt{N}}c_+^*c_-. \tag{10}$$

By having $\psi(x,0) = \sqrt{N}\phi_+^0(x) = [0, \sqrt{NL^{-1}}e^{ik_rx}]^T$ in Eqs. (7) taking the derivative of both sides of the first equation, we arrive at

$$\ddot{X} - i2\mathscr{D}\dot{X} + \omega_s^2 X(t) = -\omega_s\Omega\alpha\sqrt{N}, \tag{11a}$$

$$i\dot{\alpha} = \Delta_c\alpha + \sqrt{N}\Omega X(t) - i\kappa\alpha + i\eta, \tag{11b}$$

where $\omega_s \equiv 4\omega_r + h$, and $\omega_r \equiv \frac{k_r^2}{2m}$ is the one-photon recoil frequency. Here we can see that the dynamics of the magnetic excitation of the matter field can be mapped to that of an oscillator, for which X is the displacement. $\mathscr{D} \equiv \frac{\Omega^2 N}{2(\Delta_c - i\kappa)}$ is defined to be the viscosity constant, since it appears as a factor in the term that is of the first order in the oscillator velocity (see Eq. (11a)), signifying dissipation or friction. These equations describe a mechanical oscillator that is being coupled to the cavity field via radiation pressure.

In experiments, the cavity damping goes at the rate κ, and the eigenfrequency of X is of the order $\omega_s \sim \omega_r$ (see Eq. (11a)). Therefore, in the limit $\kappa \gg \omega_s$, the evolution of the cavity field would follow that of the matter field adiabatically [14,21]. By setting $\dot{\alpha} = 0$ for the left-hand side of Eq. (11b), we get the steady-state solution for the cavity field

$$\alpha = -\frac{i\eta + \Omega\sqrt{N}X}{(\Delta_c - i\kappa)}. \tag{12}$$

Using (12) in Eq. (11b), we have

$$\ddot{X} - i2\mathcal{D}\dot{X} + \omega_e^2 X = F, \tag{13}$$

where $F = \frac{i\sqrt{N}\omega_s\Omega\eta}{(\Delta_c - i\kappa)}$ is the radiation force of zero frequency. This equation expressly describes the motion of an oscillator moving in a viscous medium. Solving this second-order ordinary partial differential equation (ODE), we obtain

$$X(t) = \mathscr{F} - (\mathscr{F}\cos(\omega_D t) - \mathscr{C}_0\sin(\omega_D t))\,e^{i\mathscr{D}t}, \tag{14}$$

where $\mathscr{F} = F/\omega_e^2$, in which the squared frequency ω_e^2 is defined as $\omega_e^2 \equiv \omega_s^2 - \frac{N\omega_s\Omega^2}{\Delta_c - i\kappa}$. $\mathscr{C}_0$ is a constant depending on the boundary condition. $\omega_D = \sqrt{\mathscr{D}^2 + \omega_e^2}$ is the eigenfrequency of the quantum oscillator formed by the magnetic plane wave excitations.

The optomechanical motion of the magnetic excitations described by Eq. (14) shall be very traceable in experiments due to the high integrability of our light-atom coupling system. This is

Optics EXPRESS

because the photons in the cavity field participate in the atomic Bragg diffraction in a first-order process so that the equation of motion for the cavity field Eq. (11b) is an ODE of the first order in α. This enables us to map expressly the dynamics of the magnetic excitations to that of a simple mechanical oscillator (see Eq. (13)). In order to give a concrete demonstration, we use the ^{87}Rb atom and a wavelength of 852nm for the pump field [30,31] for the discussions in the rest part this article.

According to the definition (see Eq. (10)), the displacement X is complex. In Fig. 2(a), we presented the evolution of X in the time domain. It is seen that there is attenuation in amplitudes for both ReX and ImX. Some insights can be obtained by inspecting the definitions of the characteristic frequencies of the system, i.e. ω_D and $\mathscr{D}$, in the paragraph under Eq. (14). It indicates that both ω_D and $\mathscr{D}$ are complex, and this can induce a damping effect in the oscillating motion of the matter field excitations. The amplitude of the cavity field is linearly dependent on X as shown in Eq. (12) and also indicated in the data in Fig. 2(b). This exerts a strong influence on the atomic motion. Such fluctuation of the cavity field amplitude eventually results in the attenuation of the optomechanical oscillation of the magnetic excitations of the matter field. It seems that the oscillator is moving in a viscous optical medium inside the cavity with its energy being dissipated away.

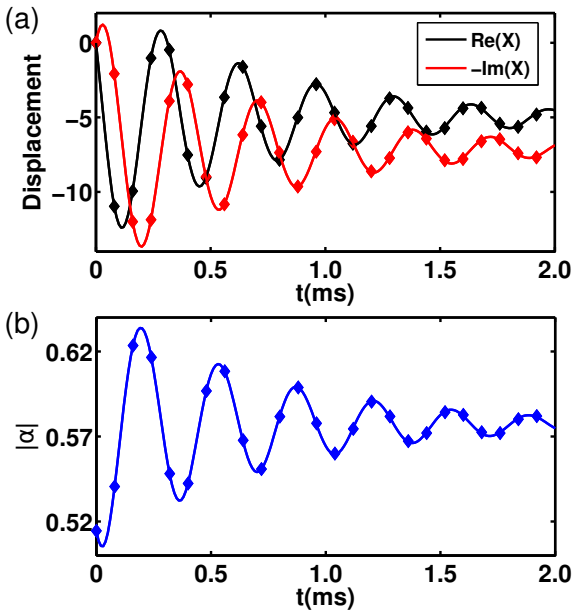

Fig. 2. (a) The evolution of the complex displacement X of the quantum oscillator consisted of the magnetic excitations of the matter field. (b) The fluctuation of the cavity field $|\alpha|$ in response to the oscillation of X. The parameters are chosen such that $N = 10^5$, $\Delta_c = 6.3 \times 10^3 \omega_r$, $\eta = \kappa = 3.7 \times 10^3 \omega_r$, $\Omega = h = 0.2\omega_r$, and $\omega_r = 2\pi \times 0.79kHz$. The solid lines are the results from the analytical solutions for the cavity field and matter field (see Eqs. (12) and (14)). The diamonds are the data from the numerical simulation with a BEC starting from a state with all the atoms condensed in the spin-up state.

In Fig. 2, there is also the result from the numerical simulation. In the simulation, a weak harmonic trap was included to provide a smooth boundary for the matter wave field. It turned out that, in a relevantly wide range of the atomic interaction strength, the results obtained by numerically integrating Eqs. (7) are in excellent agreement with Eqs. (12) and (14). This is reasonable, because if we look at the first equation of Eqs. (7), we can find that the atomic

Optics EXPRESS

interaction contributes only a constant term to the equations of motion of the matter field. Therefore, it is equivalent to a shift of the zero-point energy of the system. For this reason, we neglect the atomic interaction in the rest part of this article. Now we can conclude that the attenuation of the oscillations of the physical quantities is an intrinsic character of this CQED system. The cavity field is a viscous (instead of energy-conserving) medium for the atoms to move in. These are the very typical characteristics of the dynamics of the atoms and light in the CQED system. The dynamics predicted here is very heuristic for preparing experimental systems to further investigate the statistical properties of the matter field, which is the subject of the next section.

4. Quantum phases of the CQED system

We have seen in the last section that the magnetic excitations of the matter field in the cavity field might behave like an oscillator moving in the viscous medium in certain conditions. We can hope that this attribute of the cavity system would also intricately change the spectrum of the elementary excitations of the system and induce exotic magnetic orders for the matter field.

Now we try to get an effective Hamiltonian for the matter field by integrating out the degree of freedom of the photons. For the cavity damping being much faster than the atomic motion, we can apply the steady-sate condition for the Heisenberg equation of the cavity field, i.e. the second equation of Eqs. (6), to get

$$\hat{a} = \frac{\Omega \int dx \hat{\Psi}_+^\dagger \hat{\Psi}_- + i\eta}{(i\kappa - \Delta_c)}, \tag{15}$$

which is actually the operator counterpart of (12). When inserting the explicit form (15) into (4), we obtain

$$\hat{H}_0 = \int dx \hat{\Psi}^\dagger(x) \hat{H}_{SO} \hat{\Psi}(x) + \hat{V}. \tag{16}$$

This is the effective Hamiltonian for matter field, in which $\hat{H}_{SO}$ is defined as

$$\hat{H}_{SO} = \frac{1}{2m}(-i\partial_x + k_r\sigma_z)^2 + \Gamma\sigma_x + \frac{h}{2}\sigma_z, \tag{17}$$

where $\sigma_{x,z}$ are the two-dimensional Pauli matrices

$$\sigma_x = \begin{bmatrix} 0 & 1 \\ 1 & 0 \end{bmatrix}, \qquad \sigma_x = \begin{bmatrix} 0 & -i \\ i & 0 \end{bmatrix}.$$

$\Gamma = |\frac{i\Omega\eta}{(i\kappa - \Delta_c)}|$ is chosen to be real with an unimportant global phase having been neglected. As the index "SO" speaks for itself, $\hat{H}_0$ at this moment is in a fashion with explicit SOC. The SOC is induced by the running cavity field exchanging photons with the laser field through their interacting with the BEC, which process flips the spins of the atoms and changes the c. m. momentum of the condensate. $\hat{V}$ is the light-induced long-range exchange interaction

$$\hat{V} = g_0 \int dx dx' \hat{\Psi}_-^\dagger(x) \hat{\Psi}_+^\dagger(x') \hat{\Psi}_-(x') \hat{\Psi}_+(x), \tag{18}$$

which comes from the off-diagonal light-atom coupling. $g_0 = \frac{2N\Omega^2\Delta_c}{\kappa^2 + \Delta_c^2}$ is the interaction strength. The length of the interatomic interaction is the size of the BEC. This is because the atoms in the BEC interact with the same set of light fields; thus all the atoms are correlated with one another regardless of where they are within the condensate [32–34]. Like how the Coulomb interaction

Optics EXPRESS

transpires between the electrically charged particles in the presence of the local electromagnetic gauge field, the atoms in the CQED system exchange photons with each other and thus induce the long-range interaction. When the cavity field is red (blue)-detuned, the interaction energy is negative (positive). In this stage, even though the s-wave scattering interaction is absent, we still get an effective Hamiltonian (16) for the matter field with inter-particle interaction.

$\hat{H}_{SO}$ is the single-particle Hamiltonian of the matter field. In the picture of plane waves

$$\psi(x) = \frac{1}{\sqrt{L}} \sum_k \psi(k) e^{ikx} = \frac{1}{\sqrt{L}} \sum_k \begin{pmatrix} \psi_-(k) \\ \psi_+(k) \end{pmatrix} e^{ikx}$$

we have

$$\hat{H}_{SO} = \frac{1}{2m}(k + k_r\sigma_z)^2 + \Gamma\sigma_x + \frac{h}{2}\sigma_z. \tag{19}$$

By diagonalizing it, we get the single-particle energy

$$\omega_0(k) = \epsilon_k \pm \sqrt{\left(\delta_h\omega_r + 2\sqrt{\epsilon_k\omega_r}\right)^2 + \Gamma^2},$$

where $\epsilon_k = \frac{k^2}{2m}$ is the free-atom kinetic energy. $\delta_h = \frac{h}{\omega_r}$ is the dimensionless energy difference between $|-\rangle$ and $|+\rangle$. In the following, we are going to set δ_h as zero; this makes the system symmetric under the space- and spin-inversion transformations and thus avails much for the interesting magnetic orders to occur. There is a critical value $\Gamma_{cr}(= 2.0\omega_r)$ for Γ that, when $\Gamma<\Gamma_{cr}$, the lower branch of $\omega_0(k)$ has two minima; when $\Gamma>\Gamma_{cr}$, the lower branch has only one minimum (see Fig. 3). The wavefunction of the corresponding eigenstate is

$$\psi_k(x) = \begin{pmatrix} \psi_{k-}(x) \\ \psi_{k+}(x) \end{pmatrix} = \frac{e^{ikr}}{\sqrt{L}} \begin{pmatrix} \Gamma \\ \omega_0 - \frac{2\omega_r k}{k_r} - \delta_h - \epsilon_k \end{pmatrix}.$$

Since the interaction $\hat{V}$ is present, the system under study is very much a nonlinear system that usually doesn't have solutions in simple and compact forms. However, we can use ψ_k as a trial wavefunction, upon which we take the quantum average for $\hat{H}_0$ to get an approximation for the spectrum of the excitations of the system

$$\omega(k) = \omega_0(k) + g_0\left(\frac{\left(\omega_0(k) - \epsilon_{k-k_r} + \delta_h\right)\Gamma}{(\omega_0(k) - \epsilon_{k-k_r} + \delta_h)^2 + \Gamma^2}\right)^2. \tag{20}$$

The second term on the right-hand side is the modification of the bare atomic energy from the light-induced atomic interaction, which is noted as $V(k)$ in the following discussions.

Equation (20) is the dispersion relation of the whole CQED system. Let's dwell on it for a moment to see what we have attained, having started from the very beginning. The original CQED system is an open system with dissipation. There are photon gaining and loss in the original system described by the Hamiltonian (1). However, these two mechanisms balance out each other to help the system reach a steady stage through the multiple light fields interacting with the matter field. This steady stage is a very good platform for people to investigate the quantum statistics of the matter field in the CQED system. The energy spectrum of the system consists of two bands. At low temperatures, the lower band of the system dominates in the matter wave excitations, thus in the following we focus only on the lower branch of the spectrum of the system. In Fig. 3, we presented what $\omega(k)$ looks like under different parameter conditions. Here we need to bear in mind that each k point of the dispersion lines (the black solid lines) in this figure represents an eigenstate of the CQED system, thus there is no coupling between the

Optics EXPRESS

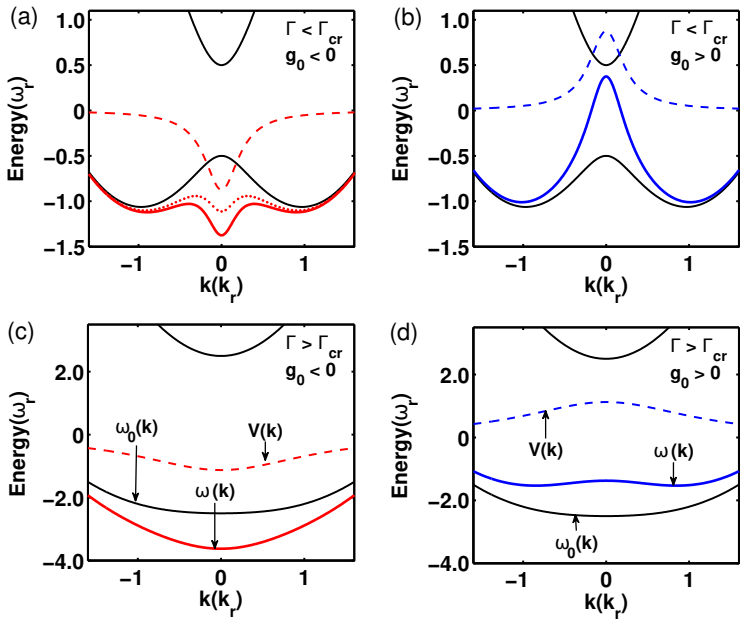

Fig. 3. The spectrum of the magnetic matter wave excitations for (a) $\Gamma = 0.5\omega_r$, $g_0 = -3.5\omega_r$, (b) $\Gamma = 0.5\omega_r$, $g_0 = 3.5\omega_r$, (c) $\Gamma = 2.5\omega_r$, $g_0 = -4.5\omega_r$, and (d) $\Gamma = 2.5\omega_r$, $g_0 = 4.5\omega_r$. The black solid lines are the bare atomic energy $\omega_0(k)$; the red (blue) dashed lines are the modification $V(k)$ upon $\omega_0(k)$ from the atomic interaction induced by the red- (blue-) detuned cavity field; the red (blue) solid lines are the combined spectrum $\omega(k)$ correspondingly. The red dotted line in (a) is a special case for $\omega(k)$ to have three minima when $g_0 = g_{cr} \approx -2.45\omega_r$; in this case, the ground state has a multi-fold degeneracy.

different k modes; each k is a quasi-momentum of the atoms in the rotated frame which should not be confused with the momentum of atoms in the laboratory frame. It can be seen that when $\Gamma \neq 0$, $\omega(k)$ is gapped. There exists a threshold g_{cr} of the strength of the atomic interaction such that when $g_0 > g_{cr}$, the lower branch of $\omega(k)$ (which will be called directly as $\omega(k)$ if there is no confusion) has two minima, and $g_0 < g_{cr}$, one, regardless of whether $\Gamma > \Gamma_{cr}$ or $\Gamma < \Gamma_{cr}$. For example, in Fig. 3(a), for a red-detuned cavity field, even though $\Gamma < \Gamma_{cr}$ so that the bare spectrum $\omega_0(k)$ has two minima for the atoms to rest on, $\omega(k)$ has only one minimum; this is because the atomic interaction $V(k)$ adds a steep dip to $\omega_0(k)$ around $k = 0$, rendering a single minimum for the whole spectrum; in this condition, the ground state of the matter field is nondegenerate. For the cavity field being blue-detuned and $\Gamma > \Gamma_{cr}$ as shown in Fig. 3(d), though $\omega_0(k)$ has only one minimum, the combined spectrum ends up with having double minima because the atomic interaction creates a strong peak centered at $k = 0$; in this condition, the ground state of the matter field still has two-fold degeneracy.

The striking point is that when g_0 approaches g_{cr}, $\omega(k)$ would develop multiple minima (more than two), because the atomic interaction induces a high nonlinearity for the system, especially for the spectrum (see Eq. (20)). As shown in Fig. 3(a) (the red dotted line), when $g = g_{cr}$, $V(k)$ is just enough to produce an extra minimum in $\omega_0(k)$, making the ground state of the matter field multi-fold degenerated.

All the characters of the interplay between the SOC and the light-induced atomic interaction can be understood in this way. The gap of the bare spectrum $\omega_0(k)$ is the narrowest at $k = 0$; therefore, the spin-up and -down components mix with each other the most at this point due to the presence of the atomic interaction, resulting in the strongest modification for the SOC and the

Optics EXPRESS

atomic energy. Hence, the light-induced long-range atomic interaction can affect the spectrum and the magnetic orders of the matter field in a drastic way.

The analysis of the spectrum of the elementary excitations of the CQED system can help us understand the potential magnetic orders of the system at low temperatures. In Fig. 4 we present a typical result from the numerical simulation for exploring the properties of the ground state of the matter field in different parameter regimes. In the numerical simulation, we use the imaginary-time evolution method to solve Eqs. (7) with the steady state condition for the cavity field $\dot{\alpha} = 0$ in the imaginary time; by doing so, we are actually solving the Hamiltonian (16) representing a closed system without dissipation. We start the evolution with an arbitrary initial seed function. Gradually, the seed function evolves into a state ψ_g with minimal energy within good accuracy for a sufficient period of time. From Fig. 4(a) through (c), the strength of the atomic interaction g_0 goes from $g_0 > g_{cr}$ to $g_0 < g_{cr}$. The left panels are ψ_g in real space, and the right panels are ψ_g in the momentum space which are obtained by Fourier transformation. We can expect that the number of peaks of $\psi_g(k)$ in the momentum space should conform with the degeneracy of the true ground state of the system under the corresponding condition. Each peak refers to an eigenmode of the ground state. We can also see that the peaks in the momentum space are slightly broadened. The major reason for this broadening is the finite-size effect due to the presence of the trapping potential. However, this does not nullify the validity of using the plane waves to expand the wavefunction of the matter field, because all the interesting quantum processes of this study take place on a length scale of the wavelength of the light fields in the CQED system. Thus the trapping potential can be regarded as constant in this tiny length scale. Therefore, plane wave expansion is still a good approximation for the system, and the quasi-momentum k is still quite a good quantum number. In the numerical simulations, we found that domains were always formed in $\psi_g(x)$ when $g_0 > g_{cr}$ as shown in Fig. 4(a1). The formation of domains is strongly dependent on the initial configuration of the seed function. The atoms cluster together to form magnetic domains. This is very similar to what happens in ferromagnetism, where one always finds a ferromagnetic state made up of locally magnetized domains. Such a phenomenon implies that ψ_g obtained is only a long-lived meta-stable state. It indicates that the true ground state of the system is degenerate like the situation of ferromagnetism with multiple magnetic domains. Actually, in each domain, the atoms lie in one of the true degenerate ground states of the CQED system. In this case, there is a spontaneous symmetry breaking (SSB) in the system. In Fig. 4(a2), there are two peaks, indicating that the true ground state is two-fold degenerate. The two degenerate states are equally favorable for the atoms to indwell; therefore, there are only two types of domains formed in the meta-stable state in Fig. 4(a1). In Fig. 4(b2) $g_0 \approx g_{cr}$, there are three major peaks, indicating that the true ground state is at least three-fold degenerate. In this case, the atoms have more low-energy states to rest on. Therefore, the long-lived meta-stable state obtained from the numerical simulation became very magnetically fragile and fractal – many tiny magnetic domains were formed spontaneously (see Fig. 4(b1)). In the case of Fig. 4(c2) $g_0 < g_{cr}$, there is only one peak, thus the ground state is nondegenerate. $\psi_g(x)$ obtained from the numerical simulation is the true ground of the system. The system is nonmagnetic (see Fig. 4(c1)) and no SSB takes place. The result here is consistent with the qualitative picture provided by the previous spectrum analysis.

Figure 5(a) is the phase diagram of the CQED system obtained by integrating Eqs. (7) in the imaginary time to gain information of the properties of the ground state of the matter field. Starting from an arbitrary seed wavefunction under the parameter condition at a given point in the phase plane, each run of the evolution of Eqs. (7) in the imaginary time yields eventually a configuration of the quantum state ψ_g that reveals the features of the true ground state of the CQED system with good precision. Each momentum peak of the state ψ_g in the momentum space tells that there is a macroscopic occupation of atoms in that momentum mode, indicating that the energy of that momentum mode is a minimum in the energy spectrum. By inspecting the

Optics EXPRESS

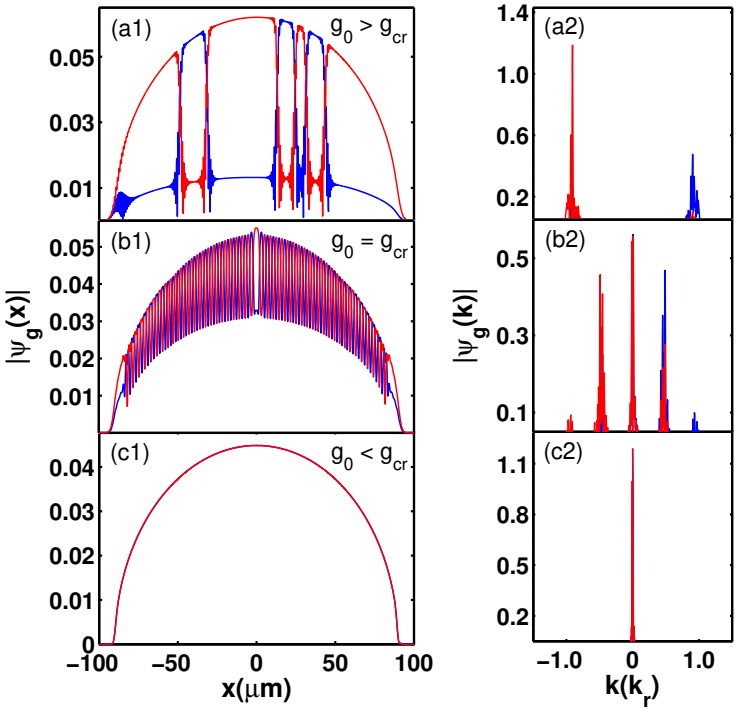

Fig. 4. The configurations for ψ_g of the matter field for $\Gamma = 1.0\omega_r$, when the strength of the atomic interaction g_0 goes from (a1-2) the parameter region $g_0 > g_{cr}$ ($g_0 = 1.0\omega_r$) to (c1-2) the $g_0 < g_{cr}$ ($g_0 = -2.0\omega_r$) region, passing through (b1-2) the critical region with $g_0 \approx g_{cr}$ ($g_0 = -1.6\omega_r$). The left panel is the profile for ψ_g in the real space, and the right panel, k-space. The red (blue) line represents the spin-down (-up) component, respectively. In (c1-2), the two spinor components coincide.

number of peaks of this wavefunction in momentum space such as Figs. 5(b)-(d), we can tell of the features of the magnetic orders in the matter field. In the small rectangles in Fig. 5(a) we present the typical profiles of the state ψ_g in coordinate space in the corresponding parameter regions. These profiles reveal the characteristics of the dispersion relation of the system. When there is quantum degeneracy in the dispersion, domains are easily formed, because the local states in different domains are degenerate with one another. When there is no degeneracy in the dispersion of the system, the ground state profile has a smooth outline. In the upper-left region of the phase diagram, the system is in the magnetic superfluid phase (MS), where ψ_g has two peaks in the momentum space indicating that there are two minima in the energy spectrum and thus the ground state is two-fold degenerate. The atoms can sit at either of these two minima; thus the ground state of the matter field breaks the $\mathbb{Z}_2$ symmetry, and the matter field would manifest the feature of the ferromagnetic materials as revealed in the previous discussions. In the bottom-right region, the matter field is in the nonmagnetic superfluid phase (NMS), in which case the spectrum has only one minimum; thus all the atoms occupy the same state of zero quasi-momentum. The atomic spins are fully mixed and cancel with each other so that the system becomes nonmagnetic and preserves the $\mathbb{Z}_2$ symmetry. The dashed line was obtained by requiring that the dispersion relation (20) has multiple minima. It serves as a boundary between the MS and NMS phases. In Table 1, we list the data which gives the relationship between the long-range interaction g_0 and the spin-orbit coupling Γ when the dispersion (20) develops multiple minima. However, the numerical simulation of imaginary time evolution gives a broadened transitional region, over

Optics EXPRESS

the whole area of which the ground state of the matter field exhibits a character of multi-fold degeneracy (MD). This broadening from the dashed line to the shaded area is partially due to the numerical uncertainty which is unavoidable in the imaginary time evolution for gaining the ground state information of the CQED system when there is quantum degeneracy, and the high nonlinearity of the CQED system should also have contributed to this. Either way, such a kind of broadening is profitable for us to observe the MD phase in experiments. At zero temperature, we expect that the MD phase appears only on the single boundary line in the parameter space (see the dashed line in Fig. 5(a)). However, practical experiments are always with a finite temperature. If the parameters are slightly off the boundary line, the CQED system would still have a weak degeneracy. The finite temperature would be well able to excite the atoms to the mode(s) with slightly higher minimum energy. Thus the three modes with minimum energy would all be macroscopically occupied. Then we are able to observe the MD phase over a finite region of the parameter space in experiments. In this MD phase, the matter field becomes magnetically unstable and fragile as was shown in Fig. 4(b) and in the relevant discussions. From Table 1 we see that $g_0<0$ when the cavity field is red-detuned ($\Delta_c<0$), and $g_0>0$ when the cavity field is blue-detuned ($\Delta_c>0$). Therefore, the quantum phase transition for the MD phase to occur is independent of whether the cavity field is red-detuned or blue-detuned. This adds abundant freedom for devising the cold atom experiments to observe this new quantum phase. Moreover, we found that the dashed line lies outside the gray area in part; this is because the dispersion relation Eq. (20) is an approximated spectrum of the excitations of the system, but the result from the numerical simulation is consistent with the dispersion relationship qualitatively and quantitatively in most part of the parameter space, showing that the results from the dispersion relation and the numerical experiment confirm with each other very well.

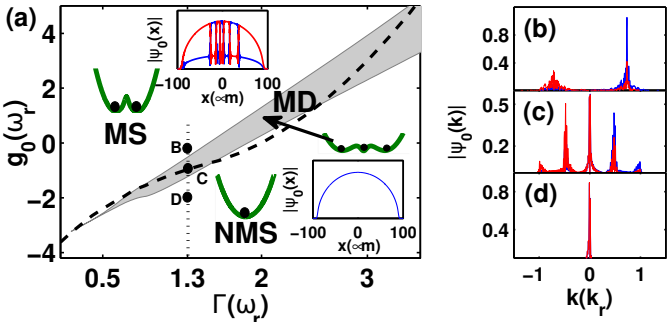

Fig. 5. (a) The phase diagram of the CQED system. The phase plane is divided into three parts, each of which is characterized by the corresponding magnetic order: the magnetic superfluid phase (noted as MS) in the upper-left plane, the transitional phase (noted as MD) with the multi-fold quantum degeneracy in the shaded area, and the nonmagnetic superfluid phase (noted as NMS) in the bottom-right region. The typical dispersion for each phase has been given for an illustration. The dashed line twining around the MD phase is the critical line on which the energy dispersion (20) has multiple minima (see Table 1 for detailed data). Each of the two rectangles demonstrates the typical profile of ψ_g obtained in the numerical experiments for learning the true ground state of the matter field in the coordinate space in the parameter region where it sits. (b), (c) and (d) are the profiles of ψ_g in the momentum space for the points B, C, and D as illustrated in (a). (The blue lines represent the data for the spin-up component, and the red ones are for the spin-down component.)

Optics EXPRESS

Table 1. The relationship between the long-range interaction g_0 and the spin-orbit coupling Γ when the MD quantum phase emerges.[a]

$\Delta_c<0$		$\Delta_c \geq 0$	
$\Gamma(\omega_r)$	$g_0<0(\omega_r)$	$\Gamma(\omega_r)$	$g_0 \geq 0(\omega_r)$
0.2	-3.27	2.0	0
0.4	-2.65	2.2	0.45
0.6	-2.17	2.4	0.97
0.8	-1.70	2.6	1.56
1.0	-1.39	2.8	2.24
1.2	-1.10	3.0	3.00
1.4	-0.85	3.2	3.84
1.6	-0.64	3.4	4.74
1.8	-0.36	3.6	5.76

[a]At this quantum phase transition, the dispersion of the CQED system develops multiple minima. The data is in the unit of the one-photon recoil frequency ω_r.

5. Discussion and conclusion

We would like to point out that the damping optomechanical motion of the elementary excitations of the CQED system is intrinsic. The physical observables, such as the number of the photons inside the cavity and the atomic occupations on the spin-up and -down states, gradually reach the steady stage after a few periods of oscillations (as shown in Fig. 2). This is very profitable for preparing a BEC in the thermal equilibrium in a real experiment by using the radio frequency technique [35], lattice shaking [36], etc. In a trap, there are discrete vibrational excited states, thus it is very necessary that the atoms be firstly cooled down to condense in the ground state of the trap to form a BEC by using cooling techniques in order to avoid the excited states being involved. Then one can turn on the lights in the CQED system so that the atoms interact with the light fields. This induces the cavity-mediated SOC and the long-range atomic interaction. Finally, by using the above artificial thermalization methods and cooling the atoms down again at the same time, we could arrive at the true ground state for the whole CQED system, and observe the quantum phase transitions in the corresponding parameter region.

The setup under our consideration is a very typical configuration of a large group of CQED systems with SOC [2,19,21]. In these systems, quantum phase transitions may take place at the double-minima to single-minimum transition of the dispersion relation under the corresponding parameter conditions. Works mentioned in Refs. [2,19] fall into this category. However, our work shows that, right at the transition point (or region), there is a new quantum phase (see the MD phase in Fig. 5) with a higher quantum degeneracy (see the red dotted line in Fig. 3(a)) and multi-fold (usually more than two folds) momentum peaks (see Fig. 4(b)) [37]. This fills the lack of relevant investigations of quantum phase transitions in the transitional area. It would add fine structures to the complete quantum phase diagrams for the CQED systems with SOC, and it would help us to dig into the salient features of the transiting behaviors of the quantum orders in these CQED systems.

Experiments can be devised to test our results. Due to the presence of the SOC, the c. m. motion of the atoms becomes relevant with the atomic spins; hence, the atoms in the spin-up and -down states with a quasi-momentum k would be found macroscopically occupying the plane wave

Optics EXPRESS

states with the momentum $k \mp k_r$ in the lab frame, respectively. Therefore, the MD quantum phase predicted in this work and the other quantum phases with the corresponding quantum degeneracy can be readily observed with the cold-atom-experiment methods, such as time-of-flight image [31] and in situ measurement [38]. The MD phase has three-fold degeneracy, thus there are usually three different momentum modes macroscopically occupied by atoms. In the time-of-flight experiment, these three different momentum modes will separate themselves from one other and be observed so that one can tell that the ground state is in the MD phase. Similarly, the MS phase is two-fold degenerate, and the NMS phase, non-degenerate. Using the time-of-flight experiment, we can determine the number of momentum modes being macroscopically occupied, and tell which quantum phase the corresponding ground state is actually in.

In conclusion, we have studied the optomechanics and the novel quantum phases of a BEC in the CQED system, which utilizes the traveling light inside a ring cavity to induce the semiquantized SOC and a highly tunable long-range atomic interaction in the matter field. We found that the motion of the magnetic excitations in the matter field can be mapped perfectly onto that of an optomechanical oscillator moving in the viscous optical medium. This optomechanical motion possesses high and exact traceability which is exempt from the influence of atomic interactions. It may find its usage in the high precision measurements [39,40] such as atomic clocks [41,42], and extensions to other hybrid systems [43]. In this system, the interrelatedness between the cavity field and the matter field is strong and nonlinear that the spectrum of the elementary excitations can be shaped into forms with diverse quantum degeneracies, especially in the transitional parameter region. This results in a new quantum phase–the MD phase which deserves our attention but has never been brought into light before. The notions and results of this work are readily realizable in experiments. They could enable new investigations in quantum optics, many-body physics, and quantum magnetism.

Funding. National Natural Science Foundation of China (11905245, 11934002, 11920101004, 91736208, 61727819); National Key Research and Development Program of China (2021YFA0718300, 2021YFA1400900); Science and Technology Major Project of Shanxi (202101030201022); Space Application System of China Manned Space Program.

Disclosures. The authors declare no conflicts of interest.

Data availability. Data underlying the results presented in this paper are not publicly available at this time but may be obtained from the authors upon reasonable request.

References

1. F. Brennecke, T. Donner, S. Ritter, T. Bourdel, M. Köhl, and T. Esslinger, "Cavity QED with a Bose–Einstein condensate," Nature **450**(7167), 268–271 (2007).
2. L. Dong, L. Zhou, B. Wu, B. Ramachandhran, and H. Pu, "Cavity-assisted Dynamical Spin-orbit Coupling in Cold Atoms," Phys. Rev. A **89**(1), 011602 (2014).
3. M. Aspelmeyer, T. J. Kippenberg, and F. Marquardt, "Cavity optomechanics," Rev. Mod. Phys. **86**(4), 1391–1452 (2014).
4. M. Asjad, P. Tombesi, and D. Vitali, "Quantum phase gate for optical qubits with cavity quantum optomechanics," Opt. Express **23**(6), 7786–7794 (2015).
5. M. Abbas, S. H. Asadpour, and H. R. Hamedi Ziauddin, "Optomechanically induced grating," Opt. Express **29**(25), 42306–42318 (2021).
6. P. Wang, Z. Yu, Z. Fu, J. Miao, L. Huang, S. Chai, H. Zhai, and J. Zhang, "Spin-Orbit Coupled Degenerate Fermi Gases," Phys. Rev. Lett. **109**(9), 095301 (2012).
7. Y. -J. Lin, K. Jimnez-Garca, and I. B. Spielman, "Spin–orbit-coupled Bose–Einstein Condensates," Nature **471**(7336), 83–86 (2011).
8. Z. Wu, L. Zhang, W. Sun, X. Xu, B. Wang, S. Ji, Y. Deng, S. Chen, X. Liu, and J. Pan, "Realization of Two-dimensional Spin-orbit Coupling for Bose-Einstein Condensates," Science **354**(6308), 83–88 (2016).
9. A. Dutt, Q. Lin, L. Yuan, M. Minkov, M. Xiao, and S. Fan, "a Single Photonic Cavity with Two Independent Physical Synthetic Dimensions," Science **367**(6473), 59–64 (2019).
10. Y-H. Lu, B-Z. Wang, and X-J. Liu, "Ideal Weyl Semimetal with 3D Spin-orbit Coupled Ultracold Quantum Gas," Sci. Bull. **65**(24), 2080–2085 (2020).
11. Y. Lei and S. Zhang, "Superradiant Phase Transition with Cavity-assisted Dynamical Spin-orbit coupling," Sci. Bull. **103**(5), 1–9 (2021).
12. K. M. Birnbaum, A. Boca, R. Miller, A. D. Boozer, T. E. Northup, and H. J. Kimble, "Photon Blockade in an Optical Cavity with One Trapped Atom," Nature **436**(7047), 87–90 (2005).

Optics EXPRESS

13. Y. Colombe, T. Steinmetz, G. Dubois, F. Linke, D. Hunger, and J. Reichel, "Strong Atom–field Coupling for Bose-Einstein Condensates in an Optical Cavity on a Chip," Nature **450**(7167), 272–276 (2007).
14. F. Brennecke, S. Ritter, T. Donner, and T. Esslinger, "Cavity Optomechanics with a Bose-Einstein Condensate," Science **322**(5899), 235–238 (2008).
15. P. Zhang, Z. Ma, J. Wu, H. Fan, and W. M. Liu, "Diffraction of Bose-Einstein Condensates in Quantized Light Fields," Phys. Rev. A **84**(1), 013614 (2011).
16. J. A. Muniz, D. Barberena, R. J. Lewis-Swan, D. J. Young, J. R. K. Cline, A. M. Rey, and J. K. Thompson, "Exploring Dynamical Phase Transitions with Cold Atoms in an Optical Cavity," Nature **580**(7805), 602–607 (2020).
17. K. Lozano-Méndez, A. H. Cásares, and S. F. Caballero-Benítez, "Spin Entanglement and Magnetic Competition via Long-Range Interactions in Spinor Quantum Optical Lattices," Phys. Rev. Lett. **128**(8), 1–7 (2022).
18. X. Zhang, Y. Chen, Z. Wu, J. Wang, J. Fan, S. Deng, and H. Wu, "Observation of a Superradiant Quantum Phase Transition in an Intracavity Degenerate Fermi Gas," Science **373**(6561), 1359–1362 (2021).
19. C. Zhu, L. Dong, and H. Pu, "Effects of Spin-orbit Coupling on Jaynes-Cummings and Tavis-Cummings Models," Phys. Rev. A **94**(5), 053621 (2016).
20. S. Gupta, K. L. Moore, K. W. Murch, and D. M. Stamper-Kurn, "Cavity Nonlinear Optics at Low Photon Numbers from Collective Atomic Motion," Phys. Rev. Lett. **99**(21), 213601 (2007).
21. Y. Deng, J. Cheng, H. Jing, and S. Yi, "Bose-Einstein Condensates with Cavity-Mediated Spin-Orbit Coupling," Phys. Rev. Lett. **112**(14), 143007 (2014).
22. D. Schmidt, H. Tomczyk, S. Slama, and C. Zimmermann, "Dynamical Instability of a Bose-Einstein Condensate in an Optical Ring Resonator," Phys. Rev. Lett. **112**(11), 115302 (2014).
23. J. Goldwin, B. P. Venkatesh, and D. H. J. O' Dell, "Backaction-Driven Transport of Bloch Oscillating Atoms in Ring Cavities," Phys. Rev. Lett. **113**(7), 073003 (2014).
24. S. Ostermann, W. Niedenzu, and H. Ritsch, "Unraveling the Quantum Nature of Atomic Self-Ordering in a Ring Cavity," Phys. Rev. Lett. **124**(3), 033601 (2020).
25. R. M. Kroeze, Y. Guo, V. D. Vaidya, J. Keeling, and B. L. Lev, "Spinor Self-Ordering of a Quantum Gas in a Cavity," Phys. Rev. Lett. **121**(16), 163601 (2018).
26. R. M. Kroeze, Y. Guo, and B. L. Lev, "Dynamical Spin-Orbit Coupling of a Quantum Gas," Phys. Rev. Lett. **123**(16), 160404 (2019).
27. M. G. Moore and P. Meystre, "Theory of Superradiant Scattering of Laser Light from Bose-Einstein Condensates," Phys. Rev. Lett. **83**(25), 5202–5205 (1999).
28. F. Dimer, B. Estienne, A. S. Parkins, and H. J. Carmichael, "Proposed Realization of the Dicke-model Quantum Phase Transition in an Optical Cavity QED System," Phys. Rev. A **75**(1), 013804 (2007).
29. K. Baumann, C. Guerlin, F. Brennecke, and T. Esslinger, "Dicke Quantum Phase Transition with a Superfluid Gas in an Optical Cavity," Nature **464**(7293), 1301–1306 (2010).
30. Z. Wang, L. Niu, P. Zhang, M. Wen, Z. Fang, X. Chen, and X. Zhou, "Asymmetric Superradiant Scattering and Abnormal Mode Amplification Induced by Atomic Density Distortion," Opt. Express **21**(12), 14377–14387 (2013).
31. Y. Zhai, P. Zhang, X. Chen, G. Dong, and X. Zhou, "Bragg Diffraction of a Matter Wave Driven by a Pulsed Nonuniform Magnetic Field," Phys. Rev. A **88**(5), 053629 (2013).
32. A. E. Niederle, G. Morigi, and H. Rieger, "Ultracold Bosons with Cavity-mediated Long-range Interactions: A Local Mean-field Analysis of the Phase Diagram," Phys. Rev. A **94**(3), 033607 (2016).
33. C. Aron, M. Kulkarni, and H. E. Türeci, "Photon-Mediated Interactions: A Scalable Tool to Create and Sustain Entangled States of *N* Atoms," Phys. Rev. X **6**(1), 1–10 (2016).
34. R. Mottl, F. Brennecke, K. Baumann, R. Landig, T. Donner, and T. Esslinger, "Roton-Type Mode Softening in a Quantum Gas with Cavity-Mediated Long-Range Interactions," Science **336**(6088), 1570–1573 (2012).
35. Y. -J. Lin, R. L. Compton, A. R. Perry, W. D. Phillips, J. V. Porto, and I. B. Spielman, "Bose-Einstein Condensate in a Uniform Light-Induced Vector Potential," Phys. Rev. Lett. **102**(13), 1 (2009).
36. C. V. Parker, L. Ha, and C. Chin, "Direct Observation of Effective Ferromagnetic Domains of Cold Atoms in a Shaken Optical Lattice," Nat. Phys. **9**(12), 769–774 (2013).
37. In [2], loop structures in the dispersion relation for the excited states were demonstrated, but there was no indication that a ground state with muti-fold quantum degeneracy and momentum peaks would appear at the transition point. Additionally, we focused only on the quantum states with the lowest energy, i.e., the ground state. Therefore, there are no loop structures showing up in the energy band in Fig. 3.
38. K. E. Wilson, Z. L. Newman, J. D. Lowney, and B. P. Anderson, "In Situ Imaging of Vortices in Bose-Einstein Condensates," Phys. Rev. A **91**(2), 023621 (2015).
39. A. Schliesser, O. Arcizet, R. Rivière, G. Anetsberger, and T. J. Kippenberg, "Resolved-sideband Cooling and Position Measurement of a Micromechanical Oscillator Close to the Heisenberg Uncertainty Limit," Nat. Phys. **5**(7), 509–514 (2009).
40. T. P. Purdy, R. W. Peterson, and C. A. Regal, "Observation of Radiation Pressure Shot Noise on a Macroscopic Object," Science **339**(6121), 801–804 (2013).
41. M. D. Swallows, M. Bishof, Y. Lin, S. Blatt, M. J. Martin, A. M. Rey, and J. Ye, "Suppression of Collisional Shifts in a Strongly Interacting Lattice Clock," Science **331**(6020), 1043–1046 (2017).
42. R. Elvin, G. W. Hoth, M. Wright, B. Lewis, J. P. McGilligan, A. S. Arnold, P. F. Griffin, and E. Riis, "Cold-atom Clock Based on a Diffractive Optic," Opt. Express **27**(26), 38359 (2019).

Optics EXPRESS

43. A. Skljarow, N. Gruhler, W. Pernice, H. Kübler, T. Pfau, R. Löw, and H. Alaeian, "Integrating Two-photon Nonlinear Spectroscopy of Rubidium Atoms with Silicon Photonics," Opt. Express **28**(13), 19593–19607 (2020).